In crystallo posttranslational modification within a MauG/pre-methylamine dehydrogenase complex

Lyndal M. R. Jensen, Ruslan Sanishvili, Victor L. Davidson and Carrie M. Wilmot

Supporting Online Material

SUPPORTING ONLINE MATERIAL

MATERIALS AND METHODS

Protein expression and purification

The methods for homologous expression of MauG in *Paracoccus denitrificans* and its purification were as described previously (*S1*). PreMADH, the biosynthetic precursor of methylamine dehydrogenase, was heterologously expressed in *Rhodobacter sphaeroides* and purified as described previously (*S2*).

Crystallization and X-ray data collection

Crystallization conditions for the MauG-preMADH complex were established using Crystal Screen (Hampton Research, CA) for vapor diffusion by the hanging drop method. Crystals were initially obtained in drops containing a 2:1 ratio (by volume) of the pre-formed protein mixture (100 μM MauG and 50 μM preMADH in potassium phosphate buffer, 10mM at pH 7.5) relative to the reservoir solution. Using the sparse matrix Crystal Screen (Hampton Research, CA), initial crystals were obtained from reagent #28 (30 % w/v PEG 8000, 0.2 M sodium acetate, 0.1 M sodium cacodylate pH 6.5). Optimization of the precipitant solution and drop contents led to reproducible crystallization in drops containing protein (1 μL)/reservoir solution mixture with ratios (by volume) of 1:2 through 1:3.5. The final crystallization conditions for the diferric MauG-preMADH complex were 24-30 % w/v PEG 8000, 0.1 M sodium acetate and 0.1 M MES pH 6.4 at 20 ˚C. Crystals appeared within a few days and were fully grown after ~ 2 weeks. Crystals were cryo-protected by including 10% PEG 400 in an artificial mother liquor equivalent to the crystallization conditions for the particular crystal. X-ray diffraction data were collected at 100K on GM/CA-CAT beamline 23-ID-B of the Advanced Photon Source (APS), Argonne National Laboratory, Argonne IL. The crystals are triclinic (P1), with unit cell parameters of a = 55.5 Å, b = 83.5 Å, c = 107.8 Å; α = 109.9°, β = 91.5°, γ = 105.8°, and one complex of 203.6 kDa (2 MauG : 1 $\alpha_2\beta_2$preMADH) in the asymmetric unit. The low symmetry of the crystals equates to a high X-ray dose to collect a complete dataset, and the diffraction resolution deteriorated significantly during the required 180^o of data collection using a 10 μm mini-beam, defined by a combination of focusing and a 10 μm aperture (*S3*). However the crystals are rods (approx. 70 μm x 15 μm x 10 μm), and this enabled the collection of multiple datasets from one crystal. When diffraction quality deteriorated (as judged by scaling statistics for processed data), the crystal was translated to a non-irradiated part and data collection continued. Four wedges of data measured from different parts of the same crystal were processed and merged with HKL2000 to compile a complete dataset (*S4*). Due to the use of the 10 μm X-ray mini-beam, a UV/visible single crystal spectrum could not be measured following diffraction data collection to assess possible X-ray induced redox changes at the MauG hemes. As the incident light beam of the UV/visible single crystal microspectrophotometer (4DX Systems AB, Sweden) has a cross-section of at least 25 μm at the crystal, significant regions of non-irradiated crystal contribute to the UV/visible spectrum. Therefore, it is not known whether the oxidation state of the heme

irons remained Fe(III) during X-ray data collection or were partially or fully reduced to Fe(II). Data collection statistics are given in Table S1.

For reaction with H_2O_2, MauG-preMADH crystals were soaked for ~ 2 minutes in a freshly prepared solution containing H_2O_2 (2 mM) in an artificial mother liquor equivalent to the crystallization conditions for the particular crystal, which also included 10 % v/v PEG 400 (the cryoprotectant). The crystals were cryo-cooled by direct transfer into liquid nitrogen and diffraction data collected at beamline 23-ID-B. The crystals diffracted to the same resolution as the untreated MauG-preMADH crystals. A different general strategy was used for data collection in this case. Even good quality protein crystals are not completely homogeneous and can have better-ordered regions (*S5*). A rastering function was used to evaluate the crystal quality throughout data collection. For the data presented here, the crystal showed good diffraction without the need to preclude any significant regions. The beam size was adjusted (w = 60 μm, h = 50 μm) to match the crystal size and orientation, and a complete 360° of diffraction data were collected. Data collection statistics are given in Table S1.

Structure solution

The crystal structure of the native MauG-preMADH complex was solved by molecular replacement into a 2.1 Å dataset using PHASER from the CCP4 program suite (*S6, S7*). Of the known di-heme CCP crystal structures, the closest sequence homolog to *P. denitrificans* MauG is di-heme CCP from *Nitrosomonas europea* (NeCCP) with 28% sequence identity, and a crystal structure solved to 1.8 Å resolution [PDB code 1IQC] (*S8*). This structure was used to generate the search model for MauG. Sequence alignments suggested some large loop insertions in MauG (Fig. S2). Therefore, a stripped-down di-heme CCP search model was used that retained only the core tertiary fold and conserved side-chains. Non-conserved amino acids and the *c*-type hemes were excluded from the model (*S1, S9*). The initial search used both the $\alpha_2\beta_2$ heterotetramer of mature PD-MADH and the heme-free NeCCP model. Following placement of the NeCCP and PD-MADH models, rigid body refinement yielded R_{work} = 42.3% (R_{free} = 42.1%). Refinement of the model was carried out using REFMAC5.5 (*S10*). During refinement no distance restraints were used between the heme irons and axial ligands. Model building and calculation of non-crystallographic symmetry (NCS) averaged electron density maps were carried out in COOT (*S11*). Two-fold NCS-averaged electron density maps were used to guide model building in the early stages, and also as restraints during refinement. Tight NCS restraints were used during refinement until most residues were located. As refinement continued, the NCS target restraints were weakened but not completely removed until the R_{work} = 18.4 % and R_{free}= 22.9 %. TLS refinement was introduced when R_{work} = 17.3 % and R_{free} = 21.8 % (*S12*). At this stage the model building was completed using electron density maps without NCS-averaging. Refinement was continued until all interpretable features of the 2Fo-Fc and Fo-Fc electron density were modeled. All the diffraction data to 2.0 Å resolution were used to calculate electron density maps and in refinement (Table S1). However due to the incompleteness in the 2.08-2.01 Å resolution shell (69%) the structure is reported as a 2.1 Å resolution structure (85% in 2.17-2.08 Å resolution shell). The final R_{work}= 13.5 % and R_{free}= 18.9 %, and the

model has good stereochemistry assessed with COOT (*S11*). The data refinement statistics are given in Table S1.

The H_2O_2-treated MauG-preMADH crystals were isomorphous to the untreated ones. Therefore, the model of the untreated protein could be refined directly against the diffraction data from the treated crystals. The reflection equivalents used to calculate R_{free} in the refinement of the untreated crystals were used to calculate R_{free} during refinement of the dataset for the H_2O_2-treated crystals. Additional reflections in the H_2O_2-treated dataset that were not measured in the untreated crystal dataset were randomly assigned to contribute either to R_{work} or R_{free}. To help prevent bias the heme models were removed, and the preMADH β-subunit residues 57 and 108 were truncated to their main-chain atoms only. Rigid body refinement with each of the six polypeptide chains defined as rigid domains gave R_{work} = 19.9 % and R_{free} = 22.7 %. The inclusion of TTQ in the model was well supported by both the 2Fo-Fc and Fo-Fc maps (Fig. 2B). Model building and restrained refinement using REFMAC5.5 with TLS until all interpretable regions of the 2Fo-Fc and Fo-Fc electron density maps were explained led to a final R_{work} = 14.2 % and R_{free} = 19.4 % (*S10*). The data refinement statistics are given in Table S1.

Enzyme characterization in solution

The MauG-dependence of TTQ synthesis by H_2O_2 has been demonstrated previously by monitoring the formation of the quinone by UV-Vis spectroscopy (*S13*). There was the possibility that components of the crystallization condition used to grow MauG-preMADH crystals might enable H_2O_2-dependent TTQ synthesis in the absence of MauG. To check for this the experiments were repeated in a medium that matched the crystal growth solution. A bulk sample of crystallization solution was prepared; 24 % w/v PEG 8000, 0.1 M MES pH 6.4 and 0.1 M sodium acetate. Stock solutions in 50 mM potassium phosphate buffer, pH 7.5 of 5 μM preMADH in the presence and absence of 0.5 μM MauG were diluted in the crystallization solution to obtain a volume ratio of 1:3 KPi to crystallization solution. A solution of 100 μM H_2O_2 was added to each sample with mixing, and the UV-Vis spectrum recorded at minute intervals. Only in the presence of MauG was TTQ formed (monitored at 440 nm) following H_2O_2 addition (Fig. S4).

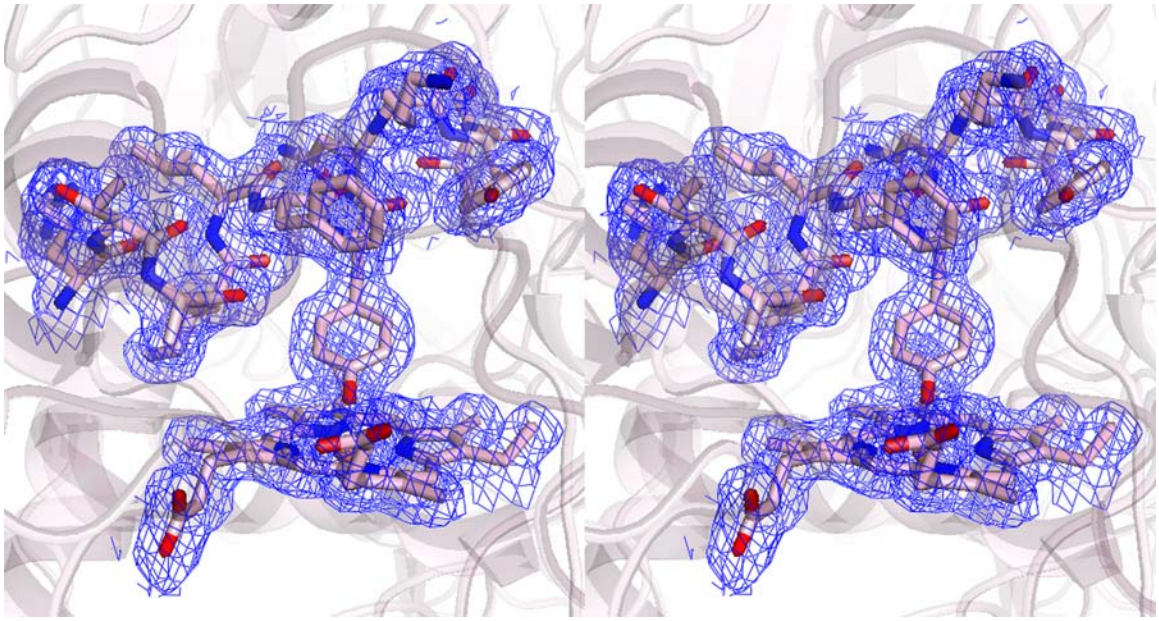

Figure S1: Wall-eye stereo image showing the quality of 2Fo-Fc electron density (contoured at 1.5 σ) within the C-terminal half of MauG. Figure produced using PyMOL (http://www.pymol.org/).

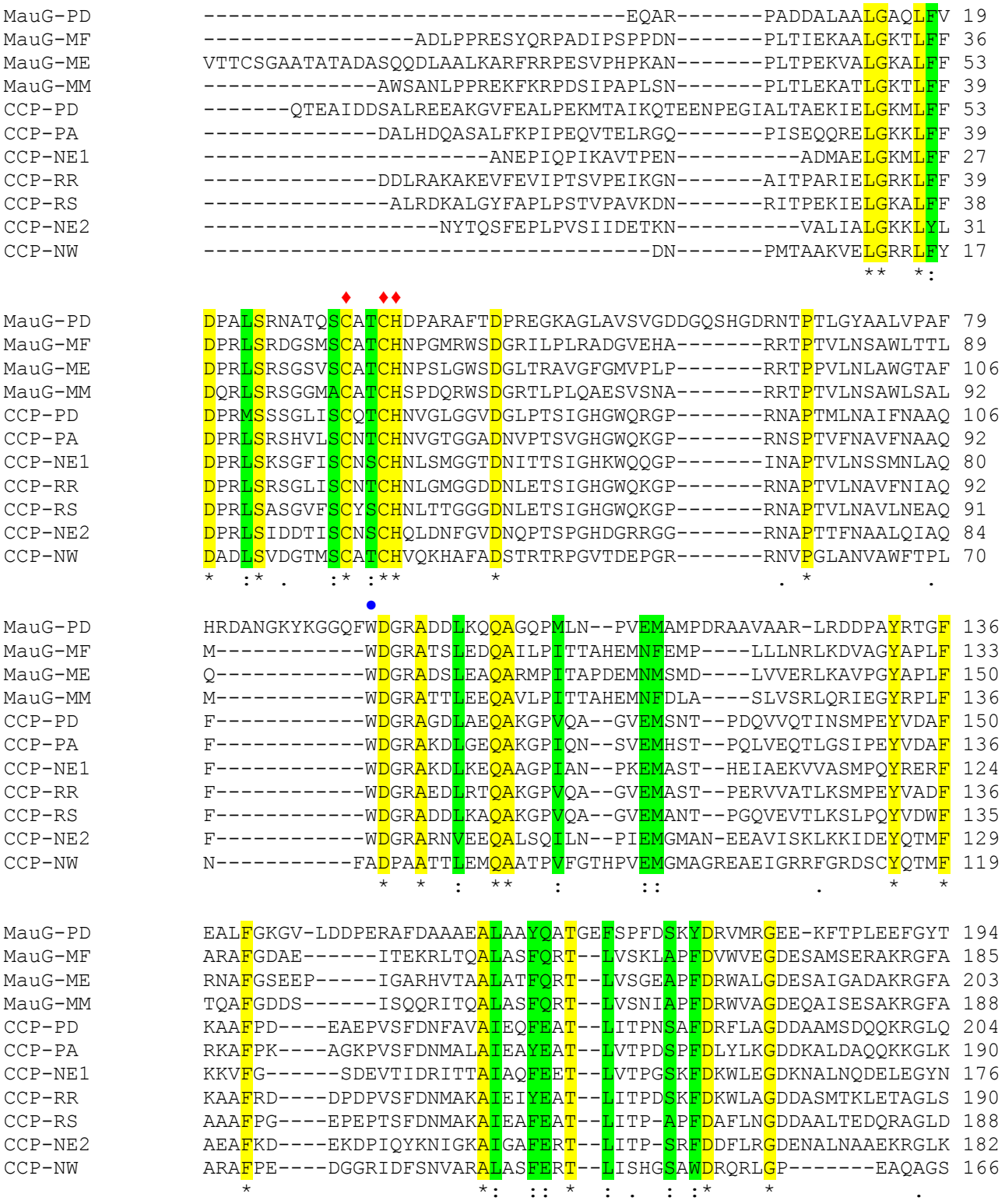
MauG-PD
MauG-MF
MauG-ME
MauG-MM
CCP-PD
CCP-PA
CCP-NE1
CCP-RR
CCP-RS
CCP-NE2
CCP-NW

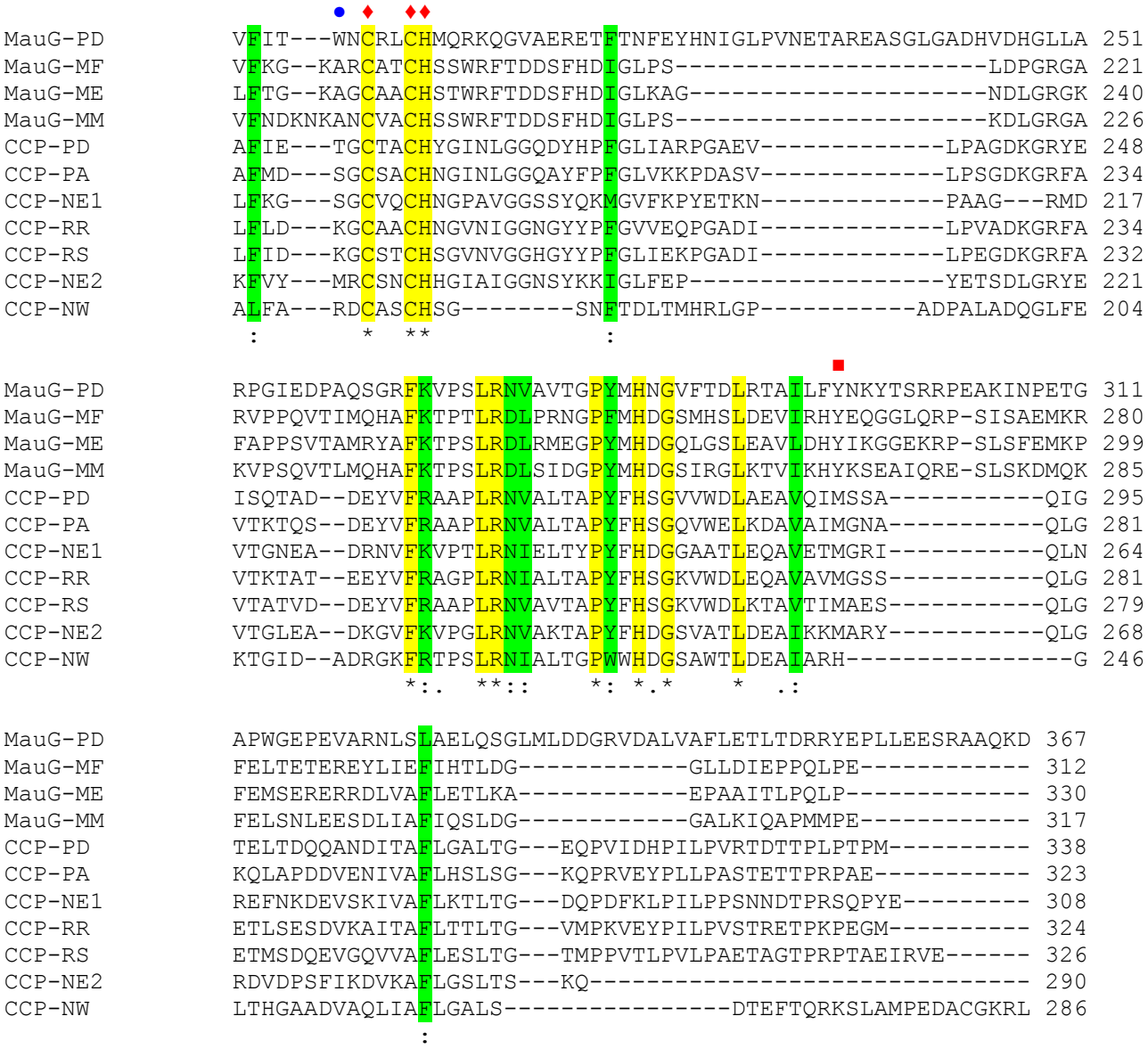
MauG-PD VFIT---WNCRLCHMQRKQGVAERETFTNFEYHNIGLPVNETAREASGLGADHVDHGLLA 251
MauG-MF VFKG--KARCATCHSSWRFTDDSFHDIGLPS----------LDPGRGA 221
MauG-ME LFTG--KAGCAACHSTWRFTDDSFHDIGLKAG----------NDLGRGK 240
MauG-MM VFNDKNKANCVACHSSWRFTDDSFHDIGLPS----------KDLGRGA 226
CCP-PD AFIE---TGCTACHYGINLGGQDYHPFGLIARPGAEV----------LPAGDKGRYE 248
CCP-PA AFMD---SGCSACHNGINLGGQAYFPFGLVKKPDASV----------LPSGDKGRFA 234
CCP-NE1 LFKG---SGCVQCHNGPAVGGSSYQKMGVFKPYETKN----------PAAG---RMD 217
CCP-RR LFLD---KGCAACHNGVNIGGNGYYPFGVVEQPGADI----------LPVADKGRFA 234
CCP-RS LFID---KGCSTCHSGVNVGGHGYYPFGLIEKPGADI----------LPEGDKGRFA 232
CCP-NE2 KFVY---MRCSNCHHGIAIGGNSYKKIGLFEP----------YETSDLGRYE 221
CCP-NW ALFA---RDCASCHSG--------SNFTDLTMHRLGP----------ADPALADQGLFE 204
MauG-PD RPGIEDPAQSGRFKVPSLRNVAVTGPYMHNGVFTDLRTAILFYNKYTSRRPEAKINPETG 311
MauG-MF RVPPQVTIMQHAFKTPTLRDLPRNGPFMHDGSMHSLDEVIRHYEQGGLQRP-SISAEMKR 280
MauG-ME FAPPSVTAMRYAFKTPSLRDLRMEGPYMHDGQLGSLEAVLDHYIKGGEKRP-SLSFEMKP 299
MauG-MM KVPSQVTLMQHAFKTPSLRDLSIDGPYMHDGSIRGLKTVIKHYKSEAIQRE-SLSKDMQK 285
CCP-PD ISQTAD--DEYVFRAAPLRNVALTAPYFHSGVVWDLAEAVQIMSSA----------QIG 295
CCP-PA VTKTQS--DEYVFRAAPLRNVALTAPYFHSGQVWELKDAVAIMGNA----------QLG 281
CCP-NE1 VTGNEA--DRNVFKVPTLRNIELTYPYFHDGGAATLEQAVETMGRI----------QLN 264
CCP-RR VTKTAT--EEYVFRAGPLRNIALTAPYFHSGKVWDLEQAVAVMGSS----------QLG 281
CCP-RS VTATVD--DEYVFRAAPLRNVAVTAPYFHSGKVWDLKTAVTIMAES----------QLG 279
CCP-NE2 VTGLEA--DKGVFKVPGLRNVAKTAPYFHDGSVATLDEAIKKMARY----------QLG 268
CCP-NW KTGID--ADRGKFRTPSLRNIALTGPWWHDGSAWTLDEAIARH----------G 246
MauG-PD APWGEPEVARNLSLAELQSGLMLDDGRVDALVAFLETLTDRRYEPLLEESRAAQKD 367
MauG-MF FELTETEREYLIEFIHTLDG----------GLLDIEPPQLPE---------- 312
MauG-ME FEMSERERRDLVAFLETLKA----------EPAAITLPQLP---------- 330
MauG-MM FELSNLEESDLIAFIQSLDG----------GALKIQAPMMPE---------- 317
CCP-PD TELTDQQANDITAFLGALTG---EQPVIDHPILPVRTDTTPLPTPM---------- 338
CCP-PA KQLAPDDVENIVAFLHSLSG---KQPRVEYPLLPASTETTPRPAE---------- 323
CCP-NE1 REFNKDEVSKIVAFLKTLTG---DQPDFKLPILPPSNNDTPRSQPYE--------- 308
CCP-RR ETLSESDVKAITAFLTTLTG---VMPKVEYPILPVSTRETPKPEGM---------- 324
CCP-RS ETMSDQEVGQVVAFLESLTG---TMPPVTLPVLPAETAGTPRPTAEIRVE------ 326
CCP-NE2 RDVDPSFIKDVKAFLGSLTS---KQ---------- 290
CCP-NW LTHGAADVAQLIAFLGALS----------DTEFTQRKSLAMPEDACGKRL 286

Figure S2: Multiple sequence alignment for MauG proteins from methylotropic and autotrophic bacteria and bacterial di-heme cytochrome *c* peroxidase proteins. Protein codes indicate the organism as follows: MauG from *Paracoccus denitrificans* (MauG-PD), *Methylobacillus flagellatus* (MauG-MF), *Methylobacterium extorquens* (MauG-ME), *Methylophilus methylotrophus* (MauG-MM); cytochrome *c* peroxidase from *Paracoccus denitrificans* (CCP-PD), *Pseudomonas aeruginosa* (CCP-PA), *Nitrosomonas europaea* (CCP-NE1), *Rhodospirillum rubrum* (CCP-RR), *Rhodobacter sphaeroides* (CCP-RS), *Nitrosomonas eutropha* (CCP-NE2), *Nitrobacter winogradskyi* (CCP-NW). Alignment was done using the ClustalW2 (Clustal 2.0.11) online program hosted by the European Bioinformatics Institute (www.ebi.ac.ak/Tools/clustalw2/index.html). Alignment selections were: matrix = blosum, gap open = 10, gap extension = 0.05 and gap distance = 8. The signal sequences were removed in accordance with either the processed signal sequences listed on the UniProt Consortium website (www.uniprot.org) or else previously reported in a published sequence alignment (*S9*). Residues that are identical in all of the sequences are indicated with an asterisk and highlighted in yellow. Residues that are of similar size and chemical properties (eg. hydrophobic, polar or acidic groupings) and/or are identical in most of the sequences are indicated with a colon and highlighted in green. Residues of similar chemical properties are indicated with a period. The CXXCH motifs that indicate the location of the *c*-type hemes are identified by red diamonds for the conserved residues (regions 31-35 and 201-205 for MauG-PD). The Tyr294 axial ligand for the six-coordinate heme of the MauG proteins (Met or His for di-heme CCP proteins) is indicated with a red square. The Trp93 and Trp199 residues that are implicated in ET in MauG-PD are indicated with blue circles.

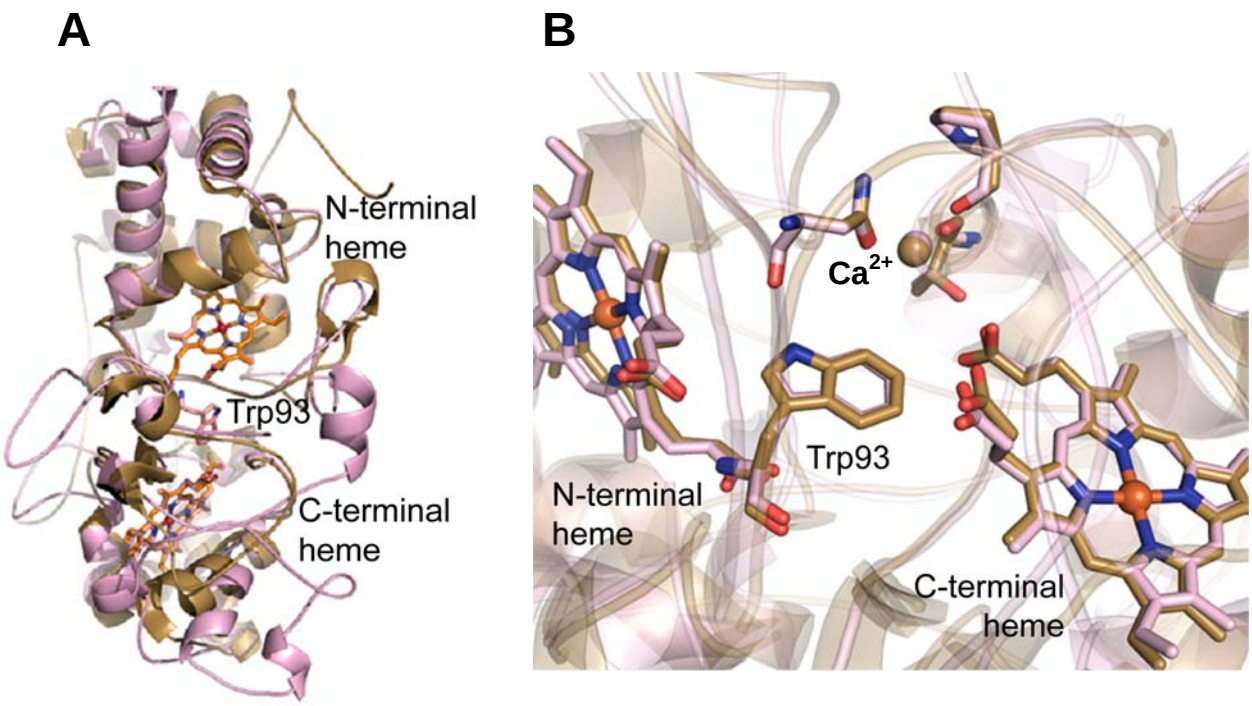

Figure S3. Overlay of MauG and *Nitrosomonas europaea* di-heme cytochrome *c* peroxidase (NeCCP). (A) Overall fold represented as a secondary structure cartoon. MauG is colored pink, NeCCP is colored gold. Hemes and intervening Trp (93 in MauG) are shown as sticks colored by element, with MauG carbons pink, and NeCCP carbons gold. Iron is shown as an orange sphere. The N-terminal and C-terminal hemes of MauG are equivalent to the peroxidatic (P-) and electron-transfer (E-) hemes respectively of di-heme CCPs. (B) Enlarged view showing the overlay of the hemes, intervening Trp93 and conserved Ca^{2+} binding site. Colors are as in panel A, with the MauG Ca^{2+} as a pink sphere, and the NeCCP Ca^{2+} gold. Figure produced using PyMOL (http://www.pymol.org/).

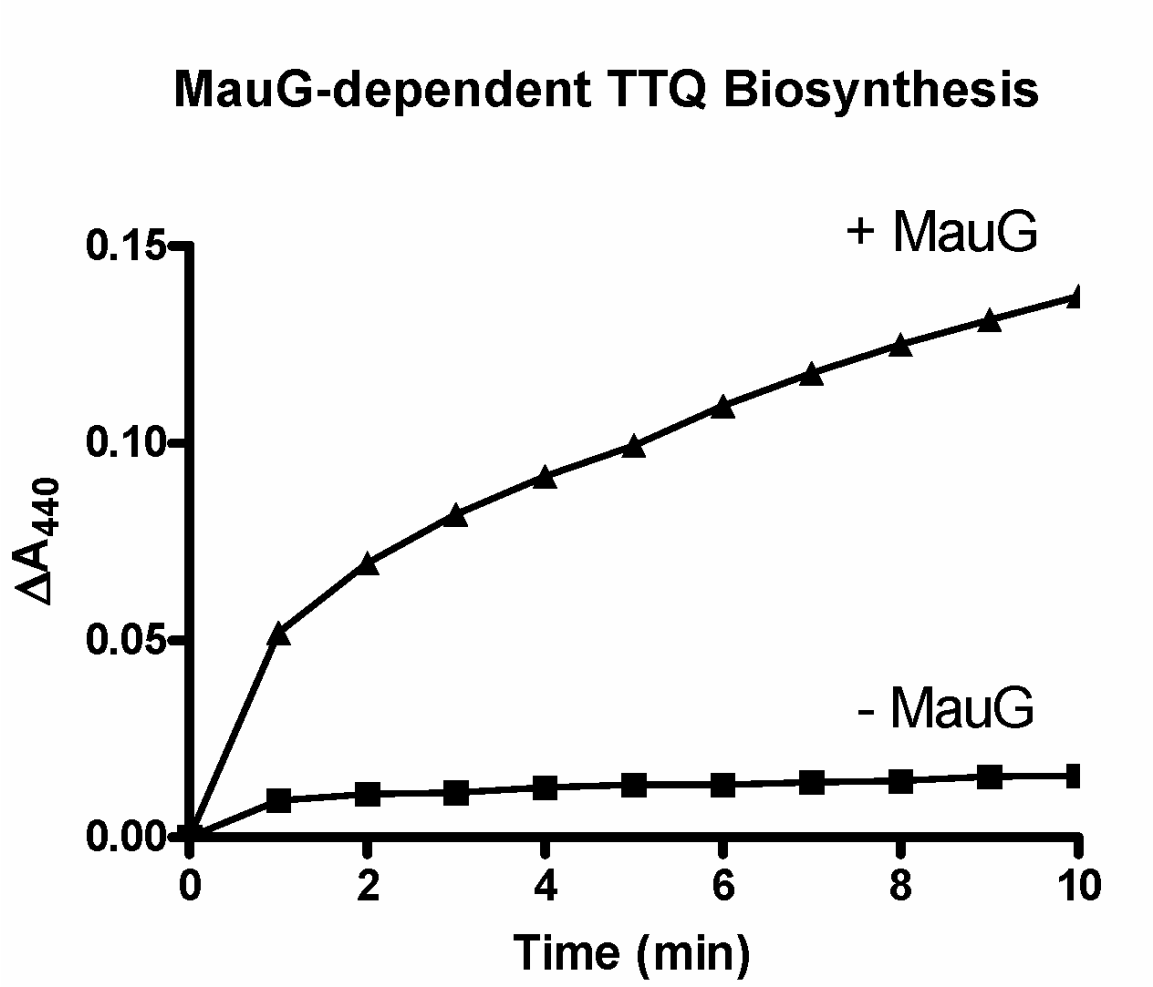

Figure S4. Time-course for MauG-dependent formation of TTQ in preMADH (monitored at 440 nm) by addition of 20-fold excess H_2O_2 in the presence of the crystallization solution. ▬■▬ MauG was absent from the solution assay. ▲▬▲ MauG was present in a 1:10 molar ratio of MauG to preMADH.

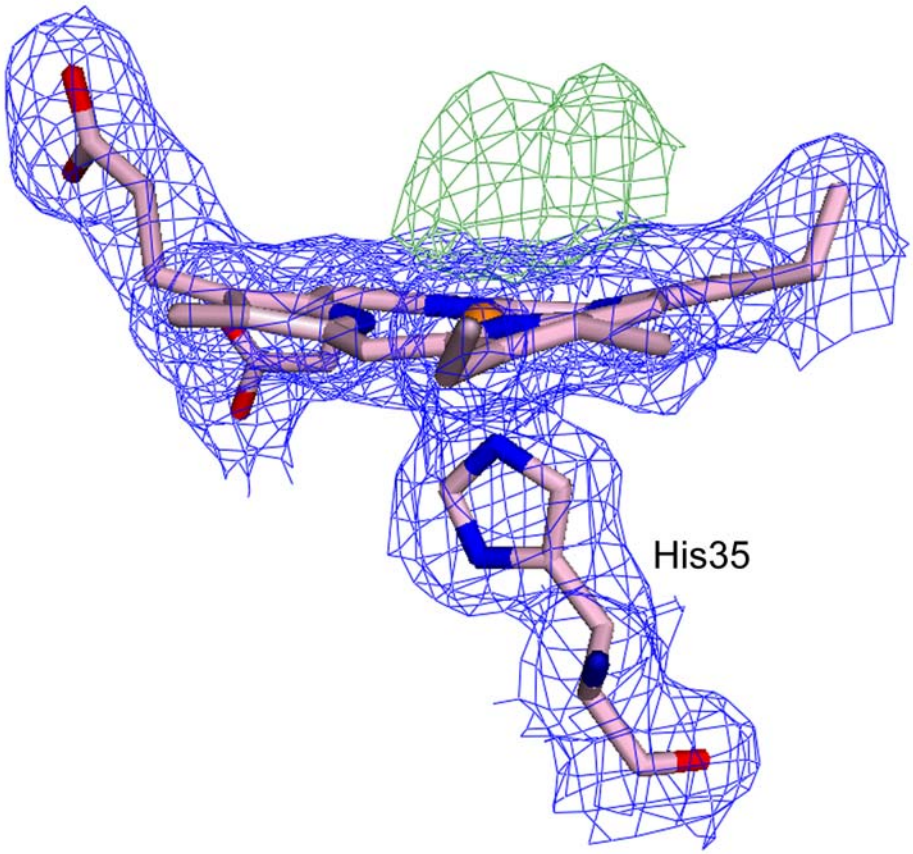

Figure S5. 2Fo-Fc (blue) and positive Fo-Fc electron density (green) at the MauG N-terminal heme (HEC500) in the MauG-preMADH + H_2O_2-treated crystal diffraction data. The 2Fo-Fc electron density is contoured at 1.5 σ, whilst the Fo-Fc is contoured at 3.0 σ. Figure produced using PyMOL (http://www.pymol.org/).

Table S1. Data collection and refinement statistics.[a]

Data collection	MauG-preMADH	H_2O_2-soaked MauG-preMADH
Detector type	MAR*mosaic* 4x4 tiled CCD	MAR*mosaic* 4x4 tiled CCD
Source	APS, Sector 23	APS, Sector 23
Space group	*P*1	*P*1
Unit cell lengths (Å)	55.53 x 83.52 x 107.78	55.53 x 83.52 x 107.78
Unit cell angles (˚)	109.94, 91.54, 105.78	109.94, 91.54, 105.78
Wavelength (Å)	1.02665	1.03320
Resolution (Å)	50.00 – 2.01 (2.08 – 2.01)	50.00 – 2.05 (2.09 – 2.05)
Measured reflections	245,905	421,716
Unique reflections	105,427	106,328
Completeness (%)	93.1 (68.6)	98.1 (97.0)
R_{merge} (%)[b]	6.7 (17.6)	7.0 (40.4)
I/σI	10.7 (4.3)	18.4 (3.4)
Multiplicity	2.3 (1.7)	4.0 (3.8)
Refinement		
Resolution (Å)	44.50 – 2.02 (2.07 – 2.02)	38.21 – 2.05 (2.10 – 2.05)
No. reflections; working/test	100,125/5,298	101,009/5,304
R_{work} (%)[c]	13.5	14.2
R_{free} (%)[d]	18.9	19.4
Protein atoms	13256	13248
Other atoms	1511	1475
Ramachandran statistics[e]		
Allowed (%)	99.29	99.29
Outliers (%)	0.71	0.71
Root mean square deviation		
Bond lengths (Å)	0.023	0.023
Bond angles (˚)	2.020	1.971
Average B-factor (Å^2)	15.17	21.83
ESU (Å)[f]; R_{work}/R_{free}	0.171/0.153	0.177/0.156

[a] Values in parentheses are for the highest resolution shell.
[b] $R_{merge} = \Sigma_i |I_{hkl,i} - \langle I_{hkl} \rangle| / \Sigma_{hkl} \Sigma_i I_{hkl,i}$, where I is the observed intensity and $\langle I_{hkl} \rangle$ is the average intensity of multiple measurements.
[c] $R_{work} = \Sigma||F_o|-|F_c|| / \Sigma|F_o|$, where $|F_o|$ is the observed structure factor amplitude, and $|F_c|$ is the calculated structure factor amplitude.
[d] R_{free} is the R factor based on 5% of the data excluded from refinement.
[e] Based on values attained from refinement validation options in COOT (*S11*).
[f] Estimated standard uncertainties generated for R_{work} and R_{free} in REFMAC5.5 (*S10*).

Table S2. Distances between potential redox centers in the MauG-preMADH complex.

Atom pairs of potential redox centers[a]	Distance (Å)[b]
5-coord. heme (HEC500)···6-coord. heme (HEC600)	
Fe···Fe	21.1
C3D···C3D (aromatic ring atoms)	14.5
O1A···O2A (closest approach)	8.7
5-coord. heme (HEC500)···MauG Trp93	
C3D···CD1 (aromatic ring atoms)	5.1
O2D···CD1 (closest approach)	3.3
6-coord. heme (HEC600)···MauG Trp93	
C3D···CZ3 (aromatic ring atoms)	5.4
O1D···CZ3 (closest approach)	3.8
5-coord. heme (HEC500)···β-preMADH Trp108	
Fe···CZ3	40.1
CHA···CZ3 (aromatic ring atoms)	37.4
O1A···CZ3 (closest approach)	32.4
6-coord. heme (HEC600)···β-preMADH Trp108	
Fe···CZ3	19.4
C3B···CZ3 (aromatic ring atoms)	15.5
CAB···CZ3 (closest approach)	14.0
6-coord. heme (HEC600)···MauG Trp199	
Fe···CE3 (closest aromatic ring atom to Fe)	12.1
Fe···CB (closest side-chain atom to Fe)	11.0
Fe···C (closest residue atom to Fe)	10.5
C3B···CE3 (aromatic ring atoms)	8.0
CAB···CB (closest approach)	5.4
MauG Trp199···β-preMADH Trp108	
NE1···CH2 (aromatic ring atoms and closest approach)	6.5
NE1···CZ3 (aromatic ring atoms and closest approach)	6.5

[a] The 5-coordinate (high-spin) and six-coordinate (low-spin) *c*-type hemes appear as HEC residues in the PDB coordinates.

[b] Distances listed are for one copy of MauG (Chain A) and its corresponding β-preMADH subunit (Chain C). Where applicable the interatomic distances are listed for the closest atom pairing between the two contributing residues.

REFERENCES

S1. Y. Wang *et al.*, *Biochemistry* **42**, 7318 (Jun 24, 2003).

S2. A. R. Pearson *et al.*, *Biochemistry* **43**, 5494 (May 11, 2004).

S3. R. F. Fischetti *et al.*, *J. Synchrotron Radiation* **16**, 217 (Mar, 2009).

S4. Z. Otwinowski, W. Minor, *Methods Enzymol.* **276**, 307 (1997).

S5. R. Sanishvili *et al.*, *Acta Crys.* **D64**, 425 (Apr, 2008).

S6. N. Collaborative Computational Project, *Acta Cryst.* **D50**, 760 (1994).

S7. A. J. McCoy *et al.*, *J. Appl. Crystallogr.* **40**, 658 (Aug 1, 2007).

S8. H. Shimizu *et al.*, *Biochemistry* **40**, 13483 (Nov 13, 2001).

S9. G. W. Pettigrew, A. Echalier, S. R. Pauleta, *J. Inorg. Biochem.* **100**, 551 (Apr, 2006).

S10. G. N. Murshudov, A. A. Vagin, E. J. Dodson, *Acta Cryst.* **D53**, 240 (May 1, 1997).

S11. P. Emsley, K. Cowtan, *Acta Cryst.* **D60**, 2126 (Dec, 2004).

S12. M. D. Winn, M. N. Isupov, G. N. Murshudov, *Acta Cryst.* **D57**, 122 (Jan, 2001).

S13. X. Li, L. H. Jones, A. R. Pearson, C. M. Wilmot, V. L. Davidson, *Biochemistry* **45**, 13276 (Nov 7, 2006).